# *Pseudomonas* mRNA 2.0: Boosting Gene Expression Through Enhanced mRNA Stability and Translational Efficiency.

**Dário Neves[1], Stefan Vos[1], Lars M. Blank[1], and Birgitta E. Ebert[1,*†]**

[1]Institute of Applied Microbiology-iAMB, Aachen Biology and Biotechnology-ABBt, RWTH Aachen University, Germany

† present address: Australian Institute for Bioengineering and Nanotechnology, The University of Queensland, Brisbane, QLD, Australia

*** Correspondence:**
Dr. Birgitta E. Ebert
birgitta.ebert@uq.edu.au

**Abstract**

High gene expression of enzymes partaking in recombinant production pathways is a desirable trait among cell factories belonging to all different kingdoms of life. High enzyme abundance is generally aimed for by utilizing strong promoters, which ramp up gene transcription and mRNA levels. Increased protein abundance can alternatively be achieved by optimizing the expression on the post-transcriptional level. Here, we evaluated protein synthesis with a previously proposed optimized gene expression architecture, in which mRNA stability and translation initiation are modulated by genetic parts such as self-cleaving ribozymes and a bicistronic design, which have initially been described to support the standardization of gene expression. The optimized gene expression architecture was tested in *Pseudomonas taiwanensis* VLB120, a promising, novel microbial cell factory. The expression cassette was employed on a plasmid basis and after single genomic integration. We used three constitutive and two inducible promoters to drive the expression of two fluorescent reporter proteins and a short acetoin biosynthesis pathway. The performance was confronted with that of a traditional expression cassette harboring the same promoter and gene of interest but lacking the genetic parts for increased expression efficiency. The optimized expression cassette granted higher protein abundance independently of the expression basis or promoter used proving its value for applications requiring high protein abundance.

**Keywords:** Synthetic Biology, ribozymes, bicistronic design, *Pseudomonas taiwanensis* VLB120, mRNA stability, high gene expression

## 1 Introduction

Cell factories have become an established role player in the sustainable production of chemicals and biological products proven with hundreds of billions of USD/year value on global markets (Davy et al., 2017). A commonality in the development of such cell factories is the continuous pursuit of

37 increased productivities through directed or selection-based genetic engineering methods. With both
38 approaches, increasing activity of the partaking pathways commonly leads to the desired rise in
39 productivity. High enzyme activity can be achieved by optimization of transcription, translation,
40 post-translational modifications, and the process conditions (Liu et al., 2013). A common strategy is
41 to employ strong promoters to overexpress product biosynthesis genes. Highly-active promoters
42 achieve increased protein production rates by increasing the respective mRNA levels in the cell.
43 However, previous studies have shown that high, recombinant gene expression leads to metabolic
44 burden and consequently to growth impairment (Borkowski et al., 2016; Carneiro et al., 2013). Such
45 hindrances are related to the drainage of biosynthetic precursors, such as nucleotides, or seizing of
46 the cellular transcriptional machinery.
47 In recent years, Synthetic Biology parts emerged that support high enzyme activities without the need
48 for strong gene expression, thereby contributing to diminishing competition and depletion of the
49 cellular mRNA pool and lightening the metabolic burden. Two translation-focused approaches can be
50 distinguished that target to optimize translation rather than transcription. To this end, the first
51 approach attempts to stabilize mRNA, whereas the second seeks to increase translational efficiency.
52 Increasing mRNA stability is possible by placing stabilizing sequences in the 5' untranslated region
53 (UTR) that avoid endoribonuclease attacks through their secondary structures as in *Escherichia coli*
54 (Carrier and Keasling, 1997; Viegas et al., 2018). The implementation of ribozymes upstream of the
55 ribosome binding site (RBS) allows the insulation of the desired expression cassette from the genetic
56 context (Lou et al., 2012). Besides the intrinsic cleaving activity, the ribozymes developed by Lou et
57 al. contained a 23 nucleotide hairpin downstream of the catalytic core, which additionally adds an
58 mRNA stabilizing trait to this genetic part (Clifton et al., 2018).
59 One approach within the second category, which focuses on translational efficiency, allows increased
60 expression levels by facilitating the access of the ribosome to the RBS. In the traditional operon
61 architecture (Figure 1A), it is possible that gene of interest (GOI)-dependent secondary structures
62 arise. This folding of the mRNA can block the access of ribosomes to the RBS thereby
63 compromising the desired gene expression (Salis et al., 2009). Mutalik et al. developed a 'bicistronic
64 design' which takes advantage of the intrinsic helicase activity of ribosomes to unveil any RBS-GOI
65 dependent secondary structure and consequently achieve GOI-independent expression (Mutalik et al.,
66 2013). In the bicistronic design, a short leading peptide cistron is allocated upstream of the GOI. The
67 RBS of the GOI is enclosed within the coding sequence of the leading cistron, whereas the start
68 codon of the GOI is fused to the stop codon of the leading cistron. The leading RBS-small peptide
69 combination is known to not create any secondary structures, which assures the binding of a
70 ribosome. Once the ribosome binds to the first RBS and starts to translate the leading peptide, any
71 possible downstream RBS-GOI dependent secondary structures are unveiled by its intrinsic helicase
72 activity exposing the RBS of the GOI. Otto et al. recently combined the bicistronic design with an
73 upstream ribozyme to increase the translational efficiency of heterologous genes integrated in rRNA
74 operons. Here the intention of the ribozyme integration was not to stabilize the mRNA but to increase
75 translation efficiency by reducing a potential steric hindrance by the bulky 5' 16S mRNA flank and
76 thereby facilitating ribosome docking. To this end, the ribozyme was placed upstream of the RBS,
77 and this integration indeed resulted in a substantial increase in protein production (Otto et al., 2019).
78 Nielsen et al. proposed the compilation of these and further genetic parts into an overall standardized
79 gene expression cassette for the assembly of genetic circuits (Figure 1B) (Nielsen et al., 2013).
80 Besides the incorporation of the gene expression parts described above, Nielsen et al. proposed the
81 isolation of the expression cassette with bidirectional terminators on both ends and the integration of
82 an RNAse III site downstream of the GOI to further reduce context-specific effects. The impact of an
83 RNAse III site downstream of the GOI was evaluated by Cambray et al. within the scope of reliable
84 terminator characterization (Cambray et al., 2013). Their extensive work showed that despite an
85 overall decrease in expression level upon RNA III site incorporation, possibly due to a shorter

86 mRNA half-life, a much narrower and precise expression level can be achieved.
87 These promoter-independent gene expression tools have been individually characterized but, to our
88 knowledge, a possible synergistic and expression enhancing effect of their combination is yet to be
89 explored.

90 In this work we constructed optimized gene expression cassettes based on the architecture proposed
91 by Nielsen et al. and evaluated the performance against traditional configurations using two
92 fluorescence proteins (msfGFP and mCherry) and recombinant acetoin production as readout
93 (Landgraf, 2012).
94 The constructed, optimized gene expression cassettes were evaluated on a plasmid basis and after
95 single-copy genomic integration (Wierckx et al., 2005). Overall, the traditional and optimized gene
96 expression cassette variants were characterized with three constitutive and two inducible promoters.
97 Reducing the overall size of the optimized gene expression cassette while maintaining its
98 performance was also targeted in this work. Besides the characterization of several constructs, qPCR
99 analysis was performed to elucidate the role of mRNA stability in altered protein expression.
100 We chose *Pseudomonas taiwanensis* VLB120 as expression host as this Gram-negative bacterium
101 exhibits industrial relevant, metabolic capabilities such as broad carbon source utilization, the ability
102 to proliferate in the presence of organic solvents, and an almost byproduct free metabolism (Köhler et
103 al., 2013; Park et al., 2007). *P. taiwanensis* VLB120 has been proven a suitable biocatalyst for the
104 production of (*S*)-styrene oxide, phenol, isobutyric acid, and 4-hydroxybenzoic acid (Lang et al.,
105 2014; Lenzen et al., 2019; Panke et al., 1998; Wynands et al., 2018). The novel expression device
106 developed in this study contributes to more effective engineering of this emergent and promising
107 biocatalysts and other prokaryotic cell factories

108

109 **2 Materials and Methods**

110 **2.1 Media and Growth Conditions**

111 Liquid cultures were grown in a horizontal rotary shaker with a shaking frequency of 200 rpm and a
112 throw of 50 mm in LB medium or LB medium supplemented with 5 g/L glucose and buffered with
113 11.64 g/L $K_2HPO_4$ and 4.89 g/L $NaH_2PO_4$ ($LB_{mod}$). *Pseudomonas* strains were grown at 30°C,
114 whereas *E. coli* was grown at 37°C. Solid LB was prepared by adding 1.5 % (w/v) agar to the
115 medium. Antibiotics were supplemented to the medium for plasmid maintenance and selection
116 purposes. Kanamycin sulfate was added at a concentration of 50 mg/L for *Pseudomonas* and *E. coli*.
117 Gentamycin was used at a concentration of 25 mg/L for both species. Tetracycline was added only to
118 solid media at a concentration of 30 mg/L for *Pseudomonas* and 10 mg/L for *E. coli*. To induce the
119 pTN1 derived plasmids harboring the *nag*R/P*nagAa* promoter system controlling the expression of
120 the fluorescent proteins or the acetoin pathway, 0.01 mM or 1 mM of sodium salicylate was added,
121 respectively. The inducer isopropyl-β-D-1 thiogalactopyranoside (IPTG) was used at a concentration
122 of 1 mM to induce the $P_{trc}$ controlled constructs integrated into the *att*Tn7 site of *Pseudomonas*
123 strains.
124 The acetoin producing strains were cultivated in airtight 500 mL serum flasks containing 50 mL of
125 $LB_{mod}$ supplemented with gentamycin (see above). The main cultures were inoculated from an
126 overnight pre-culture to an $OD_{600}$ of 0.1. The plasmid-based acetoin pathway genes were induced
127 with sodium salicylate once the cultures reached an $OD_{600}$ of 1. Afterward, samples were collected
128 for HPLC analysis.
129 The chemicals used were purchased from Merck (Darmstadt, Germany), Sigma-Aldrich (St. Louis,

130 MO, USA) or Carl Roth (Karlsruhe, Germany) unless stated otherwise. Pharmaceutical grade
131 glycerol was kindly provided by Bioeton (Kyritz, Germany).

## 132 2.2 Plasmid and strain construction

133 All plasmids were constructed through Gibson assembly (Gibson et al., 2009) using the NEBuilder
134 HiFi DNA Assembly kit (New England Biolabs, Ipswich, MA, USA). Primers used in this study
135 were purchased from Eurofins Genomics (Ebersberg, Germany) as unmodified DNA
136 oligonucleotides. PCR amplification of DNA for cloning purposes was performed using the Q5 High-
137 Fidelity Polymerase (New England Biolabs, Ipswich, MA, USA). All primers and plasmids are listed
138 in the Supplementary Information Table S1. The genes *ilvB* (from *E. coli* K-12 MG1655, Uniprot
139 P08142, with C83S mutation for improved Kcat/Km) and *aldB* (from *B. brevis*, Uniprot P23616)
140 were codon-optimized for *P. taiwanensis* VLB120 using the online tool OPTIMIZER (Puigbo et al.,
141 2007). Settings were as follows: genetic code, eubacterial; method, guided random; undesired
142 restriction sites were manually excluded, and rare codons with less than 6% usage were avoided by
143 manipulating the input codon usage table. Both codon-optimized genes and their corresponding
144 optimized gene expression parts were ordered as synthetic DNA fragments from Thermo Fisher
145 Scientific; the sequences can be found in the Supplementary Information A. The assembled plasmids
146 were transformed into either NEB® 5-alpha chemically competent *E. coli* (New England Biolabs,
147 Ipswich, MA, USA) or One Shot$^{TM}$ PIR2 Chemically Competent *E. coli* (Thermo Fisher Scientific)
148 cells through heat shock according to the supplier's protocol. Assembled plasmids were transformed
149 into *P. taiwanensis* VLB120 by electroporation using a GenePulser Xcell (BioRad, Hercules, CA,
150 USA) (settings: 2 mm cuvette gap, 2.5 kV, 200 Ω,25 µF). For DNA integration into the *att*Tn7 locus,
151 the mini-Tn7 delivery vector backbone developed by Zobel et al. (Zobel et al., 2015). was used and
152 deployed through mating procedures. For mating events, the *E. coli* donor harboring the mini-Tn7
153 vector with the constructs to be integrated, the helper strain *E. coli* HB101 pRK2013, the *E. coli* DH5
154 λpir expressing the transpose operon *tnsABCD* and the recipient strain were streaked on top of each
155 other on a LB agar plate and incubated at 30°C for 12-24 h. Further on, cell material was taken from
156 the bacterial lawn, resuspended in 0.9 % (w/v) sodium chloride solution and plated on selective
157 cetrimide agar plates. *E. coli* and *Pseudomonas* transformants were screened through colony PCR
158 using the OneTaq 2×Master Mix with standard buffer after lysing colony cell material in alkaline
159 polyethylene glycol, as described by Chomczynski and Rymaszewski.(Chomczynski and
160 Rymaszewski, 2006) Successful plasmid constructions and genome integrations were confirmed by
161 Sanger sequencing performed by Eurofins Genomics. All strains and primers used in this work are
162 shown in Table 2.

## 163 2.3 Gravimetric cell dry weight determination

164 Overnight cultures of *P. taiwanensis* VLB120 were diluted to pre-established optical densities and
165 filtered through membrane filters with a pore size of 0.2 µM which were previously weighted ($w_0$)
166 after being dried in a microwave for 3 min at 350 W. The filter cake was washed three times with
167 distilled water, dried in the microwave for 8 min at 350 W and cooled down in a desiccator before
168 weighing ($w_1$). The cell dry weight (CDW) was calculated by subtracting $w_0$ from $w_1$ and divided by
169 the volume of the filtered suspensions. 190 µL of the same cell suspensions were transferred to a 96-
170 well microtiter plate (Greiner Bio One), and scattered light signals were recorded at 620 nm with a
171 gain of 30. Linear regression between the CDW and scattered light signals of the pre-established cell
172 suspensions retrieved the conversion factor between these two units.

173

174 **2.4 Fluorescent measurements**

175 All *Pseudomonas* strains expressing fluorescent reporter proteins were characterized in the
176 microbioreactor system BioLector (m2p-labs, Baesweiler, Germany). Cultivations were performed at
177 30°C with a shaking frequency of 900 rpm and 85 % humidity in a 96-well microtiter plate (Greiner
178 Bio One) containing 190 µL of LB media supplemented with required antibiotics for plasmid
179 maintenance and sealed with evaporation reducing foil (Greiner Bio One). The main cultures were
180 inoculated from an overnight pre-culture to an $OD_{600}$ of 0.1. Growth was measured through scattered
181 light signal at 620 nm with a gain of 30, msfGFP fluorescence was excited at 485 nm and emission
182 was measured at 520 nm. The measurements were performed with gains of 50 and 70 due to signal
183 overflow of the stronger constructs. mCherry fluorescence was excited at 580 nm, and emission was
184 measured at 610 nm with a gain of 100. Scattered light values were converted into cell dry weight
185 concentrations with a predetermined calibration curve. Inducer was added to the cultures during the
186 early exponential growth phase. To allow comparison of fluorescence values recorded with different
187 gains, the msfGFP signals were converted into µM units of fluorescein, which was dissolved in 100
188 mM boric acid (See Supplementary information B for the calibration curves). Biological triplicates
189 were performed, and errors presented as the standard deviation of the mean.

190 **2.5 qPCR assays for mRNA stability assessment**

191 Biological triplicates from *P. taiwanensis* VLB120 harboring either the plasmid
192 pTN1_SPA75_Tra_GFP or pTN1_SPA75_Opt_GFP were grown overnight in $LB_{mod}$ supplemented
193 with 25 mg/mL gentamycin from a glycerol stock. On the following day, the main cultures with the
194 same medium were inoculated to an initial $OD_{600}$ of 0.1. Once the cultures reached an OD of 1, 1
195 mg/mL rifampicin and 40 µg/mL nalidixic acid were added simultaneously to cease DNA replication
196 and transcription, respectively. 2 mL samples were retrieved, centrifuged, and cell pellets flash-
197 frozen in liquid nitrogen and stored at -80°C until further sample treatment. Cell pellets were
198 suspended in 800 µL of DNA/RNA protecting buffer from the Monarch Total RNA MiniPrep kit
199 (New England Biolabs, Ipswich, MA, USA), transferred into the ZR S6012-50 Bashing beads lysis
200 tubes (Zymo Research, Irvine, CA, USA), and mechanically disrupted for 1 min. The lysate was
201 transferred into a fresh reaction tube and centrifuged for 2 min at 13,000 rpm. The supernatant was
202 transferred into a fresh tube, and the protocol proceeded as described in the Monarch Total RNA
203 MiniPrep kit. qPCR experiments with *msfGFP* and *rpoB* primers pairs were performed with 1 µL of
204 each RNA sample to confirm that the samples were not contaminated with either genomic or plasmid
205 DNA. 80 ng of RNA of each sample was converted into cDNA using the LunaScript RT SuperMix
206 kit (New England Biolabs, Ipswich, MA, USA). qPCR experiments were performed with the Luna
207 Universal qPCR Master Mix (New England Biolabs, Ipswich, MA, USA). Primer pairs efficiencies
208 for the housekeeping gene *rpoB* and target gene *msfGFP* can be seen in Supplementary Information
209 C. qPCR of samples was performed with 1 µL of the reverse transcription reaction mixtures. The
210 qPCR was performed with the CFX96 Real-Time PCR Detection System (Biorad, Hercules, CA,
211 USA). qPCR reactions were performed in technical triplicates. Absolute amounts of mRNA
212 transcripts of *msfGFP* and *rpoB* were quantified using the linear calibration curves used for primer
213 pairs efficiencies, which were constructed with either the plasmid harboring the traditional *msfGFP*
214 expression cassette under the control of the SPA75 or genomic DNA, respectively. The data was
215 analyzed with the Bio-Rad CFX Manager and Microsoft Excel software.
216 As we normalized the *msfGFP* mRNA abundance data with the transcript abundance of the
217 housekeeping gene *rpoB*, the determination of an absolute decay rate for the *msfGFP* mRNA was not
218 possible. We calculated the delta between the decay rates of the *msfGFP* and *rpoB* mRNA instead.

219 Assuming a first-order degradation kinetic for the mRNA of both genes, the time profile of the
220 normalized mRNA data can be described with Equation 1.

221
$$\frac{mRNA_{mfsGFP}(t)}{mRNA_{rpoB}(t)} = \frac{mRNA_{mfsGFP,0} \cdot exp^{k_{mfsGFP}} \cdot t}{mRNA_{rpoB,0} \cdot exp^{k_{rpoB}} \cdot t}$$

222
$$= \frac{mRNA_{mfsGFP,0}}{mRNA_{rpoB,0}} \cdot exp^{(k_{rpoB} - k_{mfsGFP}) \cdot t} \quad (Eq. 1)$$

223 A nonlinear least square algorithm was used in Matlab (The MathWorks Inc., Natick, MA, USA) to
224 fit the experimental data to Equation 1 and to determine the difference in the decay rates of the *rpoB*
225 and the *mfsGFP* gene.

226 **2.6 Analytical methods**

227 The samples taken during the acetoin producing cultivations were centrifuged at 13,000 rpm for 1
228 minute, and the supernatant was stored at -20°C until further analysis. To follow the consumption of
229 glucose and production of acetoin, a Beckman System Gold 126 Solvent Module with an organic
230 acid resin column (Polystyrene divinylbenzene copolymer (PS DVB), 300 x 8.0 mm, CS-
231 Chromatographie) was used with 5 mM $H_2SO_4$ as eluent at a flow of 0.6 mL $h^{-1}$ for 30 minutes at
232 30°C. Detection was realized with a System Gold 166 UV detector (Beckman Coulter) and a
233 Smartline RI Detector 2300 (KNAUER Wissenschaftliche Geräte, Berlin, Germany).

234

235 **3 Results and Discussion**

236 **3.1 Characterization of plasmid-based, constitutive fluorescent protein expression**

237 The optimal gene expression profile depends on the specific application. Generally, the use of robust,
238 constitutive promoters is prioritized over inducible promoters for large-scale production as they
239 render the addition of inducers unnecessary and therefore contribute the cost efficiency of microbial
240 fermentations.
241 To evaluate the impact and applicability of the consolidated, optimized expression architecture on
242 this type of promoters, we selected two synthetic promoters, Syn42 and Syn35, created by Zobel et
243 al. (originally referred to as BG42 and BG35, respectively), whereas the third one, SPA75, was
244 obtained from a synthetic promoter library created by Neves and Liebal et al. (manuscript in
245 preparation) (Zobel et al., 2015). The promoters Syn42 and SPA75 possess a rather similar and high
246 expression strength in *P. taiwanensis* VLB120, while the promoter Syn35 exhibits around 25% of the
247 expression strength of Syn42.
248 These promoters were encompassed within the optimized and traditional gene expression cassette in
249 the pTN1 plasmid backbone, a vector used by the *Pseudomonas* scientific community (Figure 2A)
250 (Schmitz et al., 2015; Verhoef et al., 2009; Wierckx et al., 2005). The optimized gene expression
251 cassette was framed between two bidirectional terminators to uncouple transcription from its genetic
252 context. For this purpose, two bidirectional terminators characterized by Chen et al., ECK120026481
253 and ECK120011170, were selected to insulate, respectively, the 5' and 3' end of the optimized gene
254 expression cassette (Chen et al., 2013). The ribozyme RiboJ, characterized by Lou et al., and the
255 bicistronic design BCD2, developed by Mutalik et al., were placed downstream of the selected
256 promoters (Lou et al., 2012; Mutalik et al., 2013). The last genetic part included was the RNAse III
257 site R1.1, characterized by Cambray et al., and placed downstream of the GOI (Cambray et al.,

258 2013). The traditional versions of the gene expression cassettes were obtained by omitting the
259 enhancing genetic parts and including the 2nd RBS of the BCD2 to maintain the ribosome affinity
260 towards the mRNA between the two expression systems (Figure 2 A).

261 The twelve constructs were evaluated in microtiter plate cultivations with online measurements of
262 fluorescence and scattered light. The scattered light values were converted into cell dry weight units,
263 whereas the arbitrary *msfGFP* fluorescence units were transformed into equivalents of fluorescein
264 (µM) to allow a direct comparison between experiments ran with different measurement settings. The
265 *mCherry* fluorescence values were not converted since all experiments were performed with the same
266 settings. However, we propose the broad implementation of such standardized fluorescence units to
267 facilitate results comparison within the scientific community. Gene expression with the different
268 constructs was characterized by the slope of the linear regression between measured fluorescence and
269 cell dry weight, which indicates a specific expression strength.

270 All optimized gene expression constructs with the three tested constitutive promoters resulted in a
271 substantial increase in fluorescence compared with their traditional counterparts (Figure 3A).
272 While the ranking of the promoter strength was maintained with the optimized gene expression
273 cassettes, absolute differences in the level of expression were reduced as a much higher increase was
274 observed for the weaker Syn35 promoter expressing mCherry (Table 1). The lower fold increase in
275 expression strength for the strong promoters suggests that the full potential of the optimized gene
276 expression cassette is not reached here because of other cellular limitations, such as RNA polymerase
277 availability.
278 In a recent study by Clifton et al.(Clifton et al., 2018) fluorescent protein expression in constructs
279 harboring a RiboJ was evaluated using 24 different, constitutive promoters covering a broad
280 spectrum of expression strength. Specific fluorescence values were not reported prohibiting a direct
281 comparison with our results. Based on the absolute GFP fluorescence values, however, no strong
282 correlation between protein expression and promoter strength was observed.

283 **3.2 Characterization of plasmid-based, inducible fluorescent protein expression**

284 Controlled gene expression is required, for instance, when the synthesis of a target product harms cell
285 fitness and needs to be decoupled from growth or in genetic circuits (Chen, 2012; Jusiak et al., 2016;
286 Terpe, 2006; Voigt, 2006). We, therefore, chose to further evaluate inducible gene expression by
287 placing the two fluorescent reporter proteins under control of the *nag*R/P*nagAa* promoter, inducible
288 with low concentrations of the relatively cheap inducer salicylate (Hüsken et al., 2001). In both, the
289 traditional and optimized expression constructs, the bidirectional terminators were left out as the first
290 attempt to reduce the overall size of the cassette. The removal of the bidirectional terminators should
291 bear similar effects in both cassettes as they have the identical genetic context. Aside from the
292 removal of the bidirectional terminators and the use of a different promoter, both expression cassettes
293 contained the equal genetic parts used for the evaluation of the constitutive promoters (Figure 2B).
294 Under the control of the inducible *nag*R/P*nagAa* promoter, the optimized gene expression cassette
295 showed a similar behavior as with the strong constitutive promoters. The specific fluorescence was
296 increased by 4-fold with the optimized gene expression cassette in comparison to their respective
297 traditional counterparts (Figure 3B). A similar increase was observed for the msfGFP signal under
298 non-induced conditions whereas for the mCherry constructs only a 2-fold increase was observed. The
299 stable increase of the msfGFP signal under both induced and uninduced conditions supports the
300 concept of a post-transcriptional gene expression enhancement. The lower fold ratio in the non-
301 induced conditions observed with the mCherry constructs could be related to analytical inaccuracies
302 of the weaker mCherry signal. Inducible promoters, such as the *nag*R/P*nagAa* promoter system used

303 in this work, tend to have a basal expression which could become problematic for the expression of
304 toxic genes or their use in systems that need to be tightly regulated, *e. g.*, genetic circuits. Attempts to
305 achieve non-leaky inducible expression systems have been made, but their number continues to be
306 limited (Horbal and Luzhetskyy, 2016). We propose the use of the optimized gene expression
307 cassette in known non-leaky inducible promoter setups to increase the available expression range in
308 such systems rather than aiming to engineer a novel non-leaky inducible variant. Since the additional
309 parts of the optimized gene expression cassette tend to act on transcribed mRNA only, an optimized
310 gene expression cassette harboring a tight, inducible promoter system could still exhibit the desired
311 non-basal expression in the absence of the inducer and, once induced, reach higher expression levels
312 than the standard counterpart.

### 313 3.3 Characterization of inducible fluorescence expression of single, genome-integrated 314 constructs

315 Genomic integration is generally preferred over plasmid-based expression when it comes to the stable
316 construction of cell factories. Integrating the pathways into the genome grants higher genetic stability
317 since it avoids common plasmid-based expression issues such as plasmid segregation and copy
318 number variability (Jahn et al., 2014; Lindmeyer et al., 2015), plasmid replication-related growth
319 impairment (Mi et al., 2016), and antibiotic dependency. However, genomic integration possesses
320 specific disadvantages like generally significantly lower expression levels and a limited number of
321 characterized integration sites (Otto et al., 2019). A common approach to overcome the low
322 expression levels of single genomic integration is to directly or randomly integrate the desired
323 expression cassette at multiple sites. However, the directed multiple integration procedure is
324 laborious and limited by the number of characterized integration sites, whereas random integration
325 requires high-throughput screening. As we had seen a significant increase in expression strength with
326 the optimized cassettes located on a plasmid, we argued that this device might also be valuable to
327 boost the output of genome-integrated constructs. To evaluate if the optimized gene expression
328 cassette could relief the low expression limitation of genomic integrations, single genomic
329 integration cassettes expressing msfGFP were constructed and integrated at the neutral *att*Tn7 site.
330 Further reduction of the optimized gene expression cassette was attempted by removing the RNAse
331 III site. As the RNAse III site does not exert a gene expression enhancement function but rather
332 contributes to its standardization, negative impact on gene expression should not be anticipated with
333 this omission.
334 To expand the promoter scope further, the standard LacI-repressed $P_{Trc}$ promoter was chosen to drive
335 the gene expression of the genome integrated cassettes. As in the plasmid-based evaluations, the
336 optimized gene expression cassette harbored the RiboJ and BCD2, whereas the traditional version
337 contained the 2$^{nd}$ RBS of the BCD2 (Figure 2C).
338 Introducing this optimized gene expression cassette in the single genomic *att*Tn7 locus yielded a ca.
339 15-fold expression increase in comparison to the traditional analog, the highest fold increase
340 observed in this work (Figure 3C). Even though RNAse III is not the major endoribonuclease
341 responsible for mRNA turnover in bacteria, the enzyme does contribute to mRNA
342 degradation.(Deutscher, 2006) By removing the RNAse III site from the optimized gene expression
343 cassette, an mRNA degradation target was abolished, which might have resulted in an increased half-
344 life of the transcripts and consequently higher expression levels.
345 The single, genome-integrated optimized expression cassette achieved expression levels of 0.098 ±
346 0.005 µmol fluorescein $g^{-1}$ cell dry weight (CDW), an expression strength in the range of the
347 plasmid-based optimized cassette under the control of the inducible promoter *nag*R/P*nagAa* or the
348 constitutive promoter Syn35 within the traditional cassette. Although the use of different promoters

349 does not allow a fair comparison, it is still noteworthy to state that expression levels were achieved
350 with the single genomic integration cassette, which are usually seen for episomally expressed genes.

### 351 3.4 Evaluation of a recombinant acetoin production pathway employing the optimized 352 expression cassette

353 Finally, a heterologous acetoin pathway was framed within the pTN1 plasmid backbone to further
354 evaluate the optimized expression cassette in a production context. The acetoin pathway included a
355 C83S mutant of the *E. coli* K-12 MG1655 acetolactate synthase (*ilvB*) and an acetolactate
356 decarboxylase (*aldB*) from *Brevibacillus brevis* (Figure 2E). The *E. coli ilv*B C83S mutant was
357 chosen due to its 4-fold lower Km and 126% higher Kcat/Km ratio compared with the wild type,
358 making it one of the most efficient enzymes of this class so far characterized (Belenky et al., 2012).
359 The *B. brevis aldB* was selected based on its low Km value (B. Rostgaard et al., 1987). In the
360 polycistronic design, expression of both genes was driven by the inducible *nag*R/P*nagAa* promoter
361 system while each gene was framed with a ribozyme, a bicistronic design version, and an RNAse III
362 site. The acetolactate synthase was framed within the VtmoJ ribozyme gene, the BCD1 bicistronic
363 design, and the RNAse III R0.5 site whereas the acetolactate decarboxylase was surrounded with the
364 RiboJ ribozyme gene, the BCD2 bicistronic design, and the RNAse III R1.1 site (Figure 2D). The
365 traditional expression cassette was obtained by removing the expression enhancing genetic parts
366 while maintaining the 2$^{nd}$ RBS of BCD1 upstream of the *ilvB* and the 2$^{nd}$ RBS of BCD2 upstream of
367 the *aldB* (Figure 2D).
368 Employing the optimized gene expression architecture to the acetoin pathway led to an acetoin
369 accumulation of 5.5 ± 0.76 mM, representing a 2.5-fold production increase when compared to the
370 traditional counterpart (Figure 3C). The increase of acetoin production solely using the optimized
371 gene expression cassette shows that its use can be extended to production contexts. The optimized
372 gene expression cassette could be advantageous for metabolic engineering approaches where high
373 gene expression is required, such as redirecting native metabolites to the desired production pathway
374 or for enzyme production for *in vitro* applications.

### 375 3.5 qPCR based elucidation of mRNA stability

376 The high fluorescence expression levels and increased acetoin production achieved by the optimized
377 gene expression in this work arose from the combination of mRNA stabilizing and translation
378 boosting genetic parts. Lou et al. integrated hairpins in both ribozymes used in this work, RiboJ and
379 VtmoJ, to expose the RBS and confirmed their catalytic functionality through rapid amplification of
380 cDNA 5'-ends.(Lou et al., 2012) The presence of such hairpins in the 5'UTR region was reported to
381 increase the respective mRNA half-life, which leads to higher protein production.(Viegas et al.,
382 2018) To evaluate if such a phenomenon occurred in the optimized gene expression cassette, qPCR
383 assays were performed to compare the decay rates of the transcripts. For this purpose, cultivations of
384 the strains expressing *msfGFP* under the control of the SPA75 promoter were treated with rifampicin
385 and nalidixic acid in the early exponential growth phase, and mRNA samples were retrieved over
386 time. The addition of rifampicin inhibits bacterial RNA polymerase, whereas nalidixic acid inhibits a
387 subunit of the DNA gyrase and topoisomerase. As the mRNA abundance data of the *mfsGFP* were
388 normalized with the data of the housekeeping gene *rpoB* to cancel out small differences in the
389 template concentration, the determination of the absolute decay rate of the *mfsGFP* transcript was not
390 possible. Instead, we calculated the difference between the decay rates of the *rpoB* and the *msfGFP*
391 mRNA (i.e., $k_{rpoB} - k_{msfGFP}$, with $k$ being the decay rate). Given that the *rpoB* mRNA decay
392 should be equal in both strains the delta can be used to reveal a possible difference in the *msfGFP*
393 decay rates in the optimized and traditional expression architecture. As hypothesized, the data was

394 significantly higher for the optimized construct (1.6-fold), which translates to a reduced decay rate of
395 the *msfGFP* transcript (Figure 4).

396 Hence, higher mRNA stability is indeed one factor contributing to the observed increase in
397 fluorescence output and acetoin production.

## 398 4 Conclusion

399 In this study, the optimized gene expression cassette architecture proposed by Nielsen et al. was
400 evaluated in *P. taiwanensis* VLB120 for the expression of fluorescent reporter genes and a 2-step
401 acetoin biosynthesis operon. The optimized gene expression cassette was characterized on a plasmid
402 or single genomic integration basis with either constitutive or inducible promoters to cover all
403 commonly used expression approaches in metabolic engineering. In all evaluations, the optimized
404 gene expression cassette outperformed its traditional counterpart. The highest improvement fold was
405 observed once the RNAse III site was removed and evaluated on a single genomic integration basis
406 under the control of the IPTG inducible $P_{Trc}$ promoter. Such a boost allowed a single genomic
407 integration-based expression to achieve expression levels commonly reached with plasmids. Within
408 the constitutive promoter paradigm, the optimized gene expression cassette increased expression
409 levels of the strongest promoter of a promoter library, showing that this tool could be used to extend
410 expression ranges further. The mRNA transcripts retrieved by the optimized gene expression
411 cassette harnessed higher stability than the transcripts from the traditional counterpart, validating that
412 mRNA stability contributed to the observed results. This work demonstrates the applicability of the
413 optimized gene expression cassette as a tool to achieve high gene expression levels through
414 transcription-independent approaches that rely on mRNA stability and translation efficiency.

## 415 5 Acknowledgments

416 We thank Maike Otto and Nick Wierckx for valuable discussions.

## 417 6 Supplementary material

418 Primers, annotated sequences of ordered DNA fragments, conversion of Biolector fluorescence a.u.
419 into µM fluorescein and qPCR primer pair efficiencies can be found in the supplementary material.

## 420 7 Author Contributions

421 DN and BEE conceived the study with the help of LMB. BEE and LMB supervised the study. DN
422 performed all experiments with the support of SV. All authors analyzed the data. All authors have
423 approved the final version of the manuscript.

## 424 8 Funding

425 This study has been conducted within the ERA SynBio project SynPath (Grant ID 031A459) with the
426 financial support of the German Federal Ministry of Education and Research.

## 427 9 Conflict of Interest

428 The authors declare that the research was conducted in the absence of any commercial or financial
429 relationships that could be construed as a potential conflict of interest.

430 **10 References**

431 B. Rostgaard, J., Svendsen, I., and Oitese, M. (1987). Isolation and characterization of an alpha-
432 acetolactate decarboxylase useful for accelerated beer maturation. in *Journal of the Institute of*
433 *Brewing* (Institute of Brewing 33 Clarges Street, London, England W1Y 8EE), 160.

434 Belenky, I., Steinmetz, A., Vyazmensky, M., Barak, Z., Tittmann, K., and Chipman, D. M. (2012).
435 Many of the functional differences between acetohydroxyacid synthase (AHAS) isozyme I and
436 other AHASs are a result of the rapid formation and breakdown of the covalent acetolactate-
437 thiamin diphosphate adduct in AHAS I. FEBS J. 279, 1967–1979. doi:10.1111/j.1742-
438 4658.2012.08577.x.

439 Borkowski, O., Ceroni, F., Stan, G. B., and Ellis, T. (2016). Overloaded and stressed: whole-cell
440 considerations for bacterial synthetic biology. Curr. Opin. Microbiol. 33, 123–130.
441 doi:10.1016/j.mib.2016.07.009.

442 Cambray, G., Guimaraes, J. C., Mutalik, V. K., Lam, C., Mai, Q. A., Thimmaiah, T., et al. (2013).
443 Measurement and modeling of intrinsic transcription terminators. Nucleic Acids Res. 41, 5139–
444 5148. doi:10.1093/nar/gkt163.

445 Carneiro, S., Ferreira, E. C., and Rocha, I. (2013). Metabolic responses to recombinant bioprocesses
446 in *Escherichia coli*. J. Biotechnol. 164, 396–408. doi:10.1016/j.jbiotec.2012.08.026.

447 Carrier, T. A., and Keasling, J. D. (1997). Engineering mRNA stability in *E. coli* by the addition of
448 synthetic hairpins using a 5′ cassette system. Biotechnol. Bioeng. 55, 577–580.
449 doi:10.1002/(SICI)1097-0290(19970805)55:3<577::AID-BIT16>3.0.CO;2-D.

450 Chen, R. (2012). Bacterial expression systems for recombinant protein production: *E. coli* and
451 beyond. Biotechnol. Adv. 30, 1102–1107. doi:10.1016/j.biotechadv.2011.09.013.

452 Chen, Y.-J., Liu, P., Nielsen, A. A. K., Brophy, J. A. N., Clancy, K., Peterson, T., et al. (2013).
453 Characterization of 582 natural and synthetic terminators and quantification of their design
454 constraints. Nat. Methods 10, 659–664. doi:10.1038/nmeth.2515.

455 Chomczynski, P., and Rymaszewski, M. (2006). Alkaline polyethylene glycol-based method for
456 direct PCR from bacteria, eukaryotic tissue samples, and whole blood. Biotechniques 40, 454–
457 458. doi:10.2144/000112149.

458 Clifton, K. P., Jones, E. M., Paudel, S., Marken, J. P., Monette, C. E., Halleran, A. D., et al. (2018).
459 The genetic insulator RiboJ increases expression of insulated genes. J. Biol. Eng. 12, 23.
460 doi:10.1186/s13036-018-0115-6.

461 Davy, A. M., Kildegaard, H. F., and Andersen, M. R. (2017). Cell Factory Engineering. Cell Syst. 4,
462 262–275. doi:10.1016/j.cels.2017.02.010.

463 Deutscher, M. P. (2006). Degradation of RNA in bacteria: Comparison of mRNA and stable RNA.
464 Nucleic Acids Res. 34, 659–666. doi:10.1093/nar/gkj472.

465 Ditta, G., Stanfield, S., Corbin, D., and Helinski, D. R. (1980). Broad host range DNA cloning
466 system for gram-negative bacteria: construction of a gene bank of *Rhizobium meliloti*. Proc.

467 Natl. Acad. Sci. 77, 7347–7351. doi:10.1073/pnas.77.12.7347.

468 Gibson, D. G., Young, L., Chuang, R. Y., Venter, J. C., Hutchison, C. A., and Smith, H. O. (2009).
469 Enzymatic assembly of DNA molecules up to several hundred kilobases. Nat. Methods 6, 343–
470 345. doi:10.1038/nmeth.1318.

471 Hanahan, D. (1985). Techniques for transformation of *E. coli*. DNA cloning a Pract. approach 1,
472 109–135. Available at: http://ci.nii.ac.jp/naid/10004787690/en/ [Accessed September 25, 2018].

473 Horbal, L., and Luzhetskyy, A. (2016). Dual control system - A novel scaffolding architecture of an
474 inducible regulatory device for the precise regulation of gene expression. Metab. Eng. 37, 11–
475 23. doi:10.1016/j.ymben.2016.03.008.

476 Hüsken, L. E., Beeftink, R., De Bont, J. A. M., and Wery, J. (2001). High-rate 3-methylcatechol
477 production in *Pseudomonas putida* strains by means of a novel expression system. Appl.
478 Microbiol. Biotechnol. 55, 571–577. doi:10.1007/s002530000566.

479 Jahn, M., Vorpahl, C., Türkowsky, D., Lindmeyer, M., Bühler, B., Harms, H., et al. (2014). Accurate
480 determination of plasmid copy number of flow-sorted cells using droplet digital PCR. Anal.
481 Chem. 86, 5969–5976. doi:10.1021/ac501118v.

482 Jusiak, B., Cleto, S., Perez-Piñera, P., and Lu, T. K. (2016). Engineering Synthetic Gene Circuits in
483 Living Cells with CRISPR Technology. Trends Biotechnol. 34, 535–547.
484 doi:10.1016/j.tibtech.2015.12.014.

485 Köhler, K. a K., Rückert, C., Schatschneider, S., Vorhölter, F. J., Szczepanowski, R., Blank, L. M., et
486 al. (2013). Complete genome sequence of *Pseudomonas* sp. strain VLB120 a solvent tolerant,
487 styrene degrading bacterium, isolated from forest soil. J. Biotechnol. 168, 729–730.
488 doi:10.1016/j.jbiotec.2013.10.016.

489 Landgraf, D. (2012). Quantifying Localizations and Dynamics in Single Bacterial Cells. Available at:
490 https://dash.harvard.edu/handle/1/9920184?show=full.

491 Lang, K., Zierow, J., Buehler, K., and Schmid, A. (2014). Metabolic engineering of *Pseudomonas* sp.
492 strain VLB120 as platform biocatalyst for the production of isobutyric acid and other secondary
493 metabolites. Microb. Cell Fact. 13, 2. doi:10.1186/1475-2859-13-2.

494 Lenzen, C., Wynands, B., Otto, M., Bolzenius, J., Mennicken, P., Blank, L. M., et al. (2019). High-
495 Yield Production of 4-Hydroxybenzoate From Glucose or Glycerol by an Engineered
496 *Pseudomonas taiwanensis* VLB120. Front. Bioeng. Biotechnol. 7, 1–17.
497 doi:10.3389/fbioe.2019.00130.

498 Lindmeyer, M., Jahn, M., Vorpahl, C., Müller, S., Schmid, A., and Bühler, B. (2015). Variability in
499 subpopulation formation propagates into biocatalytic variability of engineered *Pseudomonas*
500 *putida* strains. Front. Microbiol. 6, 1–15. doi:10.3389/fmicb.2015.01042.

501 Liu, L., Yang, H., Shin, H., Chen, R. R., Li, J., Du, G., et al. (2013). How to achieve high-level
502 expression of microbial enzymes Strategies and perspectives © 2013 Landes Bioscience . Do
503 not distribute. Bioengineered 4, 212–223. doi:10.4161/bioe.24761.

504 Lou, C., Stanton, B., Chen, Y.-J., Munsky, B., and Voigt, C. A. (2012). Ribozyme-based insulator
505 parts buffer synthetic circuits from genetic context. Nat. Biotechnol. 30, 1137–42.
506 doi:10.1038/nbt.2401.

507 Martínez-García, E., and de Lorenzo, V. (2011). Engineering multiple genomic deletions in Gram-
508 negative bacteria: Analysis of the multi-resistant antibiotic profile of *Pseudomonas putida*
509 KT2440. Environ. Microbiol. 13, 2702–2716. doi:10.1111/j.1462-2920.2011.02538.x.

510 Mi, J., Sydow, A., Schempp, F., Becher, D., Schewe, H., Schrader, J., et al. (2016). Investigation of
511 plasmid-induced growth defect in *Pseudomonas putida*. J. Biotechnol. 231, 167–173.
512 doi:10.1016/j.jbiotec.2016.06.001.

513 Mutalik, V. K., Guimaraes, J. C., Cambray, G., Lam, C., Christoffersen, M. J., Mai, Q.-A., et al.
514 (2013). Precise and reliable gene expression via standard transcription and translation initiation
515 elements. Nat. Methods 10, 354–60. doi:10.1038/nmeth.2404.

516 Nielsen, A. a K., Segall-Shapiro, T. H., and Voigt, C. a. (2013). Advances in genetic circuit design:
517 Novel biochemistries, deep part mining, and precision gene expression. Curr. Opin. Chem. Biol.
518 17, 878–892. doi:10.1016/j.cbpa.2013.10.003.

519 Otto, M., Wynands, B., Drepper, T., Jaeger, K.-E., Thies, S., Loeschcke, A., et al. (2019). Targeting
520 16S ribosomal DNA for stable recombinant gene expression in *Pseudomonas*. ACS Synth. Biol.,
521 acssynbio.9b00195. doi:10.1021/acssynbio.9b00195.

522 Panke, S., Witholt, B., Schmid, a, and Wubbolts, M. G. (1998). Towards a biocatalyst for (*S*)-styrene
523 oxide production: characterization of the styrene degradation pathway of *Pseudomonas* sp.
524 strain VLB120. Appl Env. Microbiol 64, 2032–2043.

525 Park, J.-B., Bühler, B., Panke, S., Witholt, B., and Schmid, A. (2007). Carbon metabolism and
526 product inhibition determine the epoxidation efficiency of solvent-tolerant *Pseudomonas* sp.
527 strain VLB120ΔC. Biotechnol. Bioeng. 98, 1219–1229. doi:10.1002/bit.21496.

528 Puigbo, P., Guzman, E., Romeu, A., and Garcia-Vallve, S. (2007). OPTIMIZER: a web server for
529 optimizing the codon usage of DNA sequences. Nucleic Acids Res. 35, W126–W131.
530 doi:10.1093/nar/gkm219.

531 Salis, H. M., Mirsky, E. A., and Voigt, C. A. (2009). Automated design of synthetic ribosome
532 binding sites to control protein expression. Nat. Biotechnol. 27, 946–950. doi:10.1038/nbt.1568.

533 Schmitz, S., Nies, S., Wierckx, N., Blank, L. M., and Rosenbaum, M. A. (2015). Engineering
534 mediator-based electroactivity in the obligate aerobic bacterium *Pseudomonas putida* KT2440.
535 Front. Microbiol. 6, 1–13. doi:10.3389/fmicb.2015.00284.

536 Terpe, K. (2006). Overview of bacterial expression systems for heterologous protein production:
537 From molecular and biochemical fundamentals to commercial systems. Appl. Microbiol.
538 Biotechnol. 72, 211–222. doi:10.1007/s00253-006-0465-8.

539 Verhoef, S., Wierckx, N., Westerhof, R. G. M., De Winde, J. H., and Ruijssenaars, H. J. (2009).
540 Bioproduction of p-hydroxystyrene from glucose by the solvent-tolerant bacterium
541 *Pseudomonas putida* S12 in a two-phase water-decanol fermentation. Appl. Environ. Microbiol.

542 75, 931–936. doi:10.1128/AEM.02186-08.

543 Viegas, S. C., Apura, P., Martínez-García, E., De Lorenzo, V., and Arraiano, C. M. (2018).
544 Modulating Heterologous Gene Expression with Portable mRNA-Stabilizing 5′-UTR
545 Sequences. ACS Synth. Biol. 7, 2177–2188. doi:10.1021/acssynbio.8b00191.

546 Voigt, C. A. (2006). Genetic parts to program bacteria. Curr. Opin. Biotechnol. 17, 548–557.
547 doi:10.1016/j.copbio.2006.09.001.

548 Wierckx, N. J. P., Ballerstedt, H., de Bont, J. A. M., and Wery, J. (2005). Engineering of Solvent-
549 Tolerant *Pseudomonas putida* S12 for Bioproduction of Phenol from Glucose. Appl. Environ.
550 Microbiol. 71, 8221–8227. doi:10.1128/AEM.71.12.8221-8227.2005.

551 Wynands, B., Lenzen, C., Otto, M., Koch, F., Blank, L. M., and Wierckx, N. (2018). Metabolic
552 engineering of *Pseudomonas taiwanensis* VLB120 with minimal genomic modifications for
553 high-yield phenol production. Metab. Eng. 47, 121–133. doi:10.1016/j.ymben.2018.03.011.

554 Zobel, S., Benedetti, I., Eisenbach, L., de Lorenzo, V., Wierckx, N., and Blank, L. M. (2015). Tn7-
555 Based Device for Calibrated Heterologous Gene Expression in *Pseudomonas putida*. ACS
556 Synth. Biol. 4, 1341–1351. doi:10.1021/acssynbio.5b00058.

557

558 **11 Tables**

559 **Table 1.** Pairwise fold-changes of specific fluorescence (fluorescence per g cell dry weight) between
560 the optimized and traditional gene expression cassettes calculated as described by Clifton et al
561 (Clifton et al., 2018).

| Expression System | pTN1 plasmid | | | | -*att*Tn7:: |
|---|---|---|---|---|---|
| Promoter | Syn35 | Syn42 | SPA75 | *nagR*/P*nagAa* | *lacI*$^{Q}$/P$_{Trc}$ |
| msfGFP | 8.7±1.6 | 5.0±0.9 | 3.9±0.3 | 4.1±0.7 | 14.7±1.6 |
| mCherry | 11.3±3.8 | 3.8±0.2 | 2.9±0.4 | 3.9±0.7 | - |

562

563 **Table 2.** Strains used in this study.

| Strain | Description | References |
|---|---|---|
| *E. coli* | | |
| DH5a | *supE44*, *ΔlacU169* (*φ80lacZΔM15*), *hsdR17* (rK−mK +), *recA1*, *endA1*, *gyrA96*, *thi-1*, *relA1* | (Hanahan, 1985) |
| PIR2 | F- Δ*lac169 rpoS*(Am) *robA1 creC510 hsdR514 endA recA1 uidA*(ΔMluI)::*pir* | Thermo Scientific |
| HB101 pRK2013 | Sm$^{R}$, *hsdR-M*$^{+}$, *proA2*, *leuB6*, *thi-1*, *recA*; bears plasmid pRK2013 | (Ditta et al., 1980) |
| DH5a pSW-2 | DH5α bearing pSW-2 | (Martínez-García and de Lorenzo, 2011) |

| | | |
|---|---|---|
| DH5aλpir pTNS1 | DH5αλpir bearing plasmid pTNS1 | (Martínez-García and de Lorenzo, 2011) |
| *P. taiwanensis* | | |
| VLB120 | Wild type | (Panke et al., 1998) |
| VLB120 pTN1_Syn35_T_GFP | bearing plasmid pTN1_SynPro35_Tra_GFP | This study |
| VLB120 pTN1_Syn35_O_GFP | bearing plasmid pTN1_SynPro35_Opt_GFP | This study |
| VLB120 pTN1_Syn35_T_mCherry | bearing plasmid pTN1_SynPro35_Tra_mCherry | This study |
| VLB120 pTN1_Syn35_O_mCherry | bearing plasmid pTN1_SynPro35_Opt_mCherry | This study |
| VLB120 pTN1_Syn42_T_GFP | bearing plasmid pTN1_SynPro42_Tra_GFP | This study |
| VLB120 pTN1_Syn42_O_GFP | bearing plasmid pTN1_SynPro42_Opt_GFP | This study |
| VLB120 pTN1_Syn42_T_mCherry | bearing plasmid pTN1_SynPro42_Tra_mCherry | This study |
| VLB120 pTN1_Syn42_O_mCherry | bearing plasmid pTN1_SynPro42_Opt_mCherry | This study |
| VLB120 pTN1_SPA75_T_GFP | bearing plasmid pTN1_SPA75_Tra_GFP | This study |
| VLB120 pTN1_SPA75_O_GFP | bearing plasmid pTN1_SPA75_Opt_GFP | This study |
| VLB120 pTN1_SPA75_T_mCherry | bearing plasmid pTN1_SPA75_Tra_mCherry | This study |
| VLB120 pTN1_SPA75_O_mCherry | bearing plasmid pTN1_SPA75_Opt_mCherry | This study |
| VLB120 pTN1_*nagR*_T_GFP | bearing plasmid pTN1_*nagR*_Tra_GFP | This study |
| VLB120 pTN1_*nagR*_O_GFP | bearing plasmid pTN1_*nagR*_Opt_GFP | This study |
| VLB120 pTN1_*nagR*_T_mCherry | bearing plasmid pTN1_n*agR*_Tra_mCherry | This study |
| VLB120 pTN1_*nagR*_O_mCherry | bearing plasmid pTN1_*nagR*_Opt_mCherry | This study |
| VLB120 *att*Tn7::IPTG_T_GFP | *att*Tn7::tetA_IPTG_Tra_GFP | This study |
| VLB120 *att*Tn7::IPTG_O_GFP | *att*Tn7::tetA_IPTG_Opt_GFP | This study |
| VLB120 pTN1_*nagR*_T_acetoin | bearing plasmid pTN1_*nagR*_Tra_ilvB_aldB | This study |
| VLB120 pTN1_*nagR*_O_acetoin | bearing plasmid pTN1_n*agR*_Opt_ilvB_aldB | This study |

## 12 Figure legends

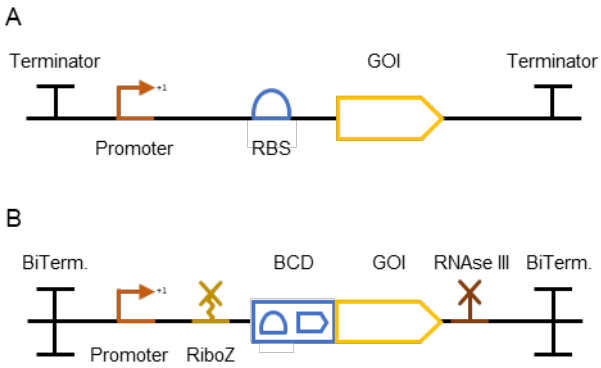


**Figure 1.** Gene expression cassette architectures represented with glyphs compliant with Synthetic Biology Open Language Visual (SBOLv). (A) A traditional gene expression cassette comprising a promoter, an RBS, and a gene of interest (GOI), (B) an optimized gene expression cassette as proposed by Nielsen et al., framed between two bidirectional terminators (Bi. term.) and encompassing a promoter, a ribozyme (RiboZ), the bicistronic design (BCD) developed by Mutalik et al.(Mutalik et al., 2013), a GOI and an RNAse III site.

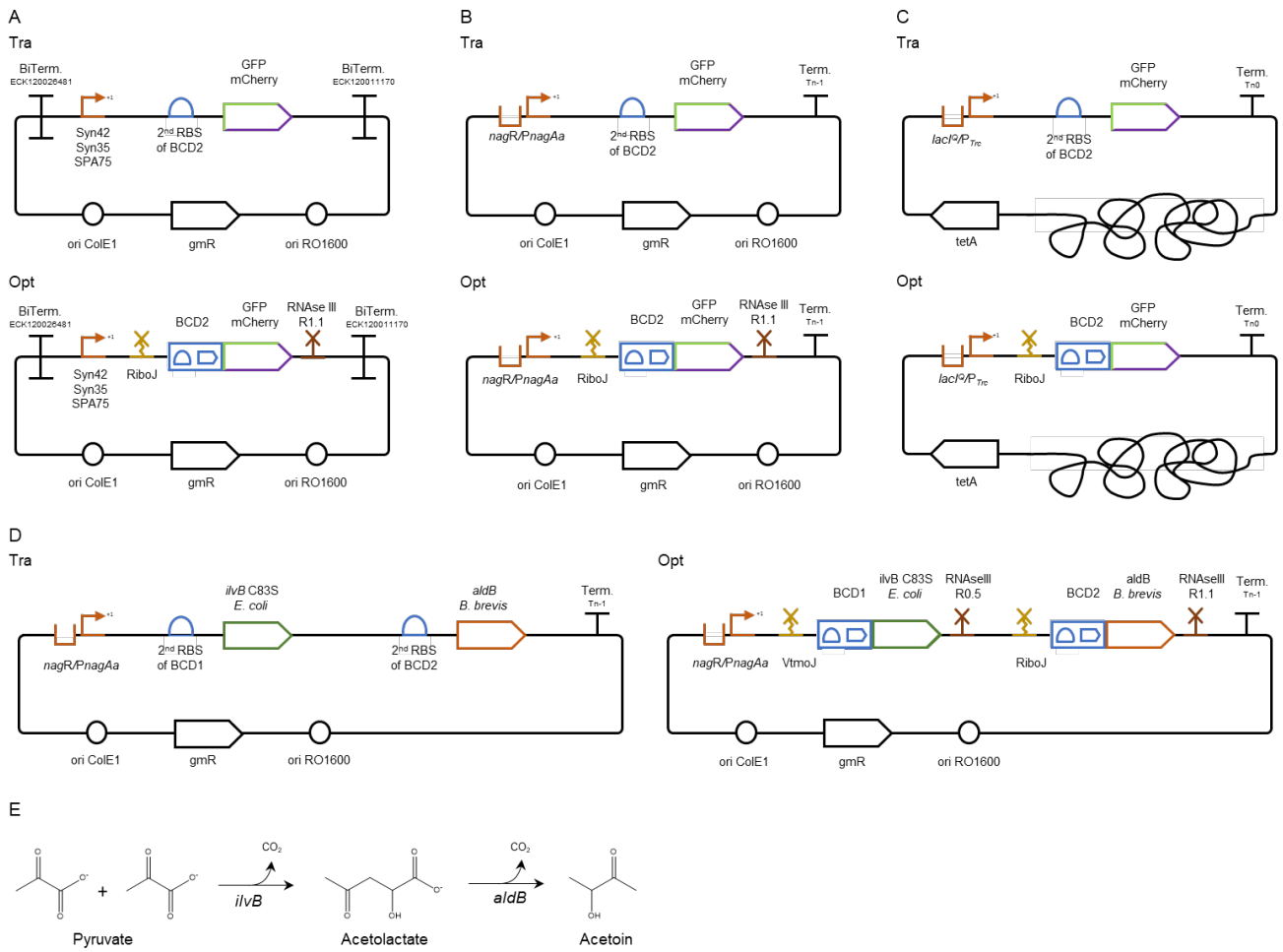


**Figure 2.** Gene expression constructs evaluated within this work. Traditional and optimized gene expression cassettes for (A) the plasmid-based evaluation of the expression of two fluorescent reporters (msfGFP and mCherry) under the control of three constitutive promoters (Syn42, Syn35, and SPA75) and (B) the salicylate inducible PnagAa promoter; (C) Traditional and optimized gene expression cassettes for single genomic integration into the attTn7 site. The expression with these constructs was evaluated using the fluorescent reporter msfGFP under the control of the IPTG inducible PTrc promoter; (D) traditional and optimized gene expression cassettes for the plasmid-based evaluation of an acetoin pathway under the control of the salicylate inducible PnagAa promoter, (E) acetoin pathway comprising the C83S ilvB mutant from E. coli and aldB from Brevibacillus brevis; Tra, traditional gene expression cassette; Opt, optimized gene expression cassette; RBS, ribosomal binding site; Bi. term., bidirectional terminator; BCD, bicistronic design; VtmoJ, RiboJ, synthetic ribozyme; RNAseIII R1.1 and R0.5, RNase III restriction sites; *gmR*, gentamycin resistance gene; *tetA*, tetracycline resistance gene; ori ColE1 and ori RO1600, origins of replication.

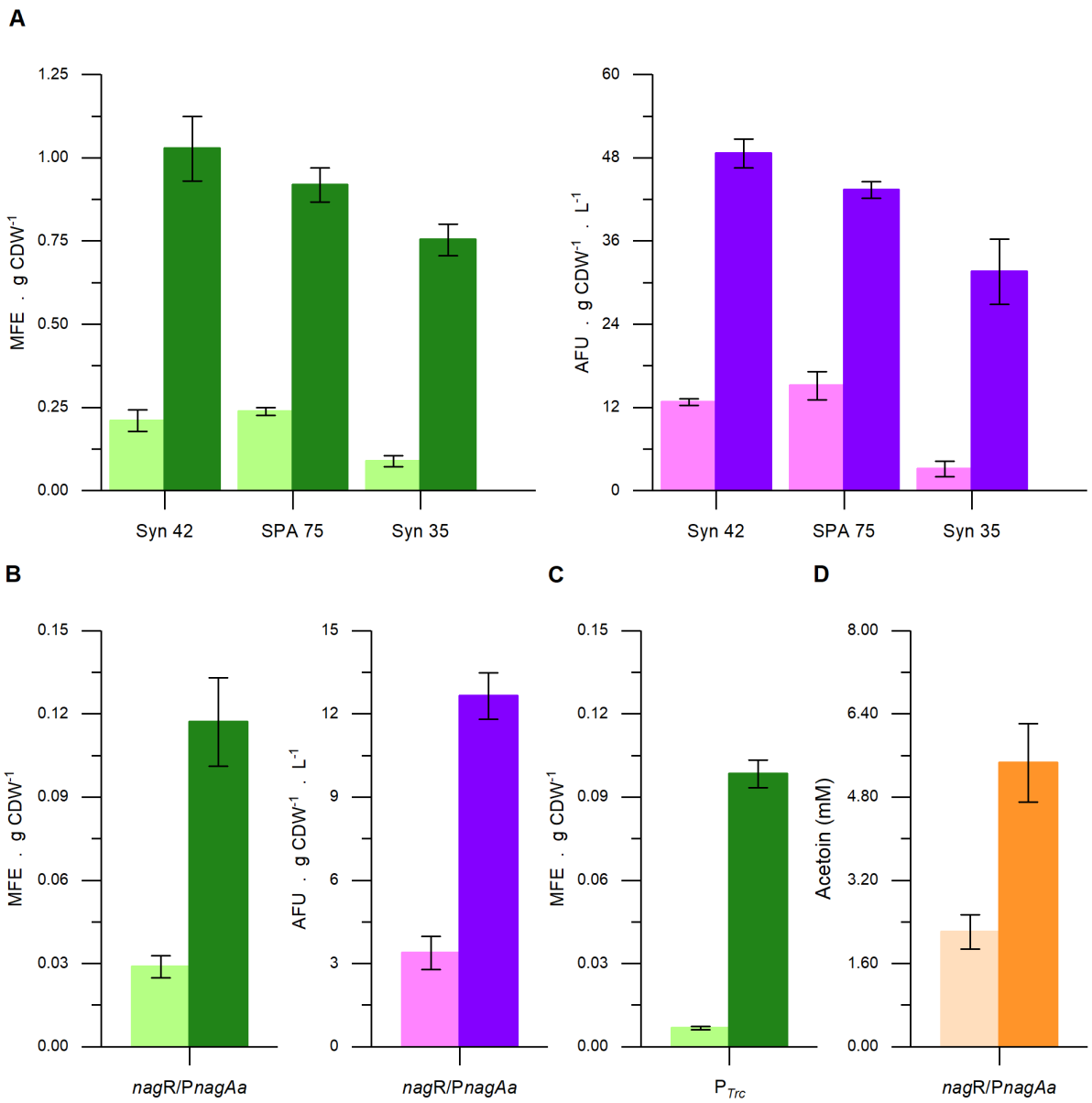


**Figure 3.** Evaluation of the developed gene expression constructs: plasmid-based expression of msfGFP (green) and mCherry (pink) with the traditional (light-colored) or optimized (dark-colored) expression cassette employing (A) constitutive and (B) the inducible P*nagAa* promoter, (C) mfsGFP expression under the control of the inducible $P_{Trc}$ promoter from single copies of the traditional and optimized gene expression cassettes integrated into the *att*Tn7 site, (D) plasmid-based expression of an acetoin pathway under the control of the inducible P*nagAa* promoter employing a traditional and an optimized expression cassette Error bars indicate the standard deviation of three biological replicates except for the inducible *nag*R/P*nagAa* construct expressing mCherry in which biological

597 duplicates are represented. CDW, cell dry weight. Abbreviations: MFE, µmoles of fluorescein
598 equivalents; AFU, arbitrary fluorescence units.

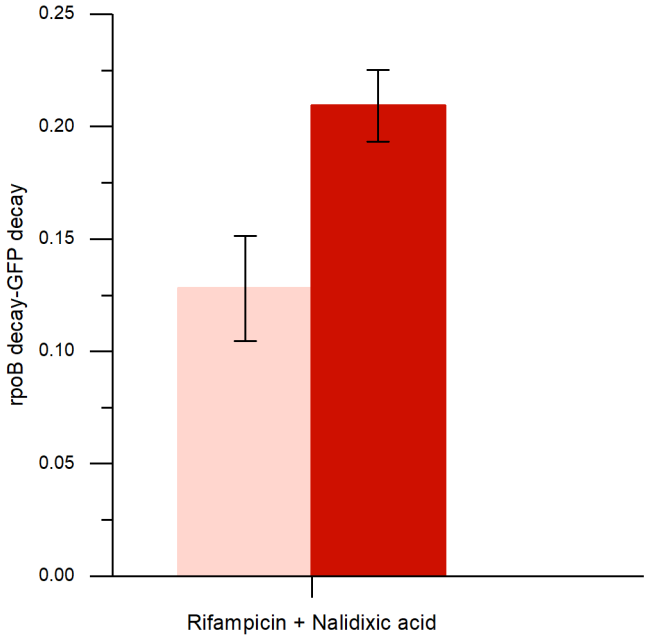


599

600 **Figure 4.** qPCR based elucidation of mRNA stability of *msfGFP* transcripts from the plasmid-based
601 traditional (light-colored) and optimized (dark-colored) expression cassettes harboring the
602 constitutive SPA75 promoter. Early exponential cultivations were treated with the antibiotics,
603 nalidixic acid and rifampicin, to halt DNA replication and transcription, respectively. Samples were
604 taken over time, and mRNA levels were assessed through qPCR. mRNA decay rates of transcripts
605 from each expression cassette were retrieved through the difference between the decay rate of the
606 housekeeping gene *rpoB* and the target *msfGFP*. Error bars indicate the standard deviation of two
607 biological replicates.

608

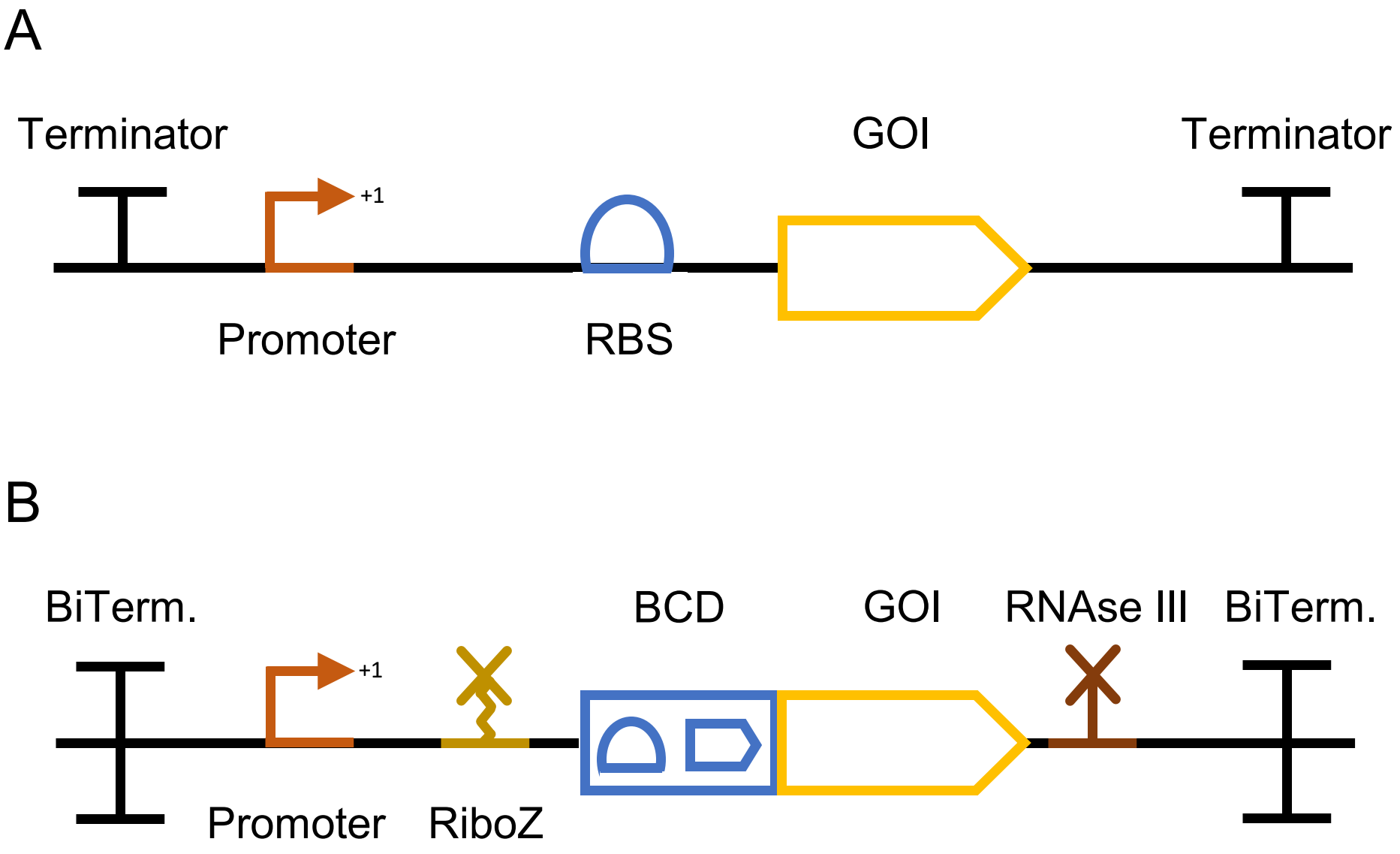
A
Terminator
GOI
Terminator
+1
Promoter
RBS
B
BiTerm.
BCD
GOI
RNAse III
BiTerm.
+1
Promoter
RiboZ

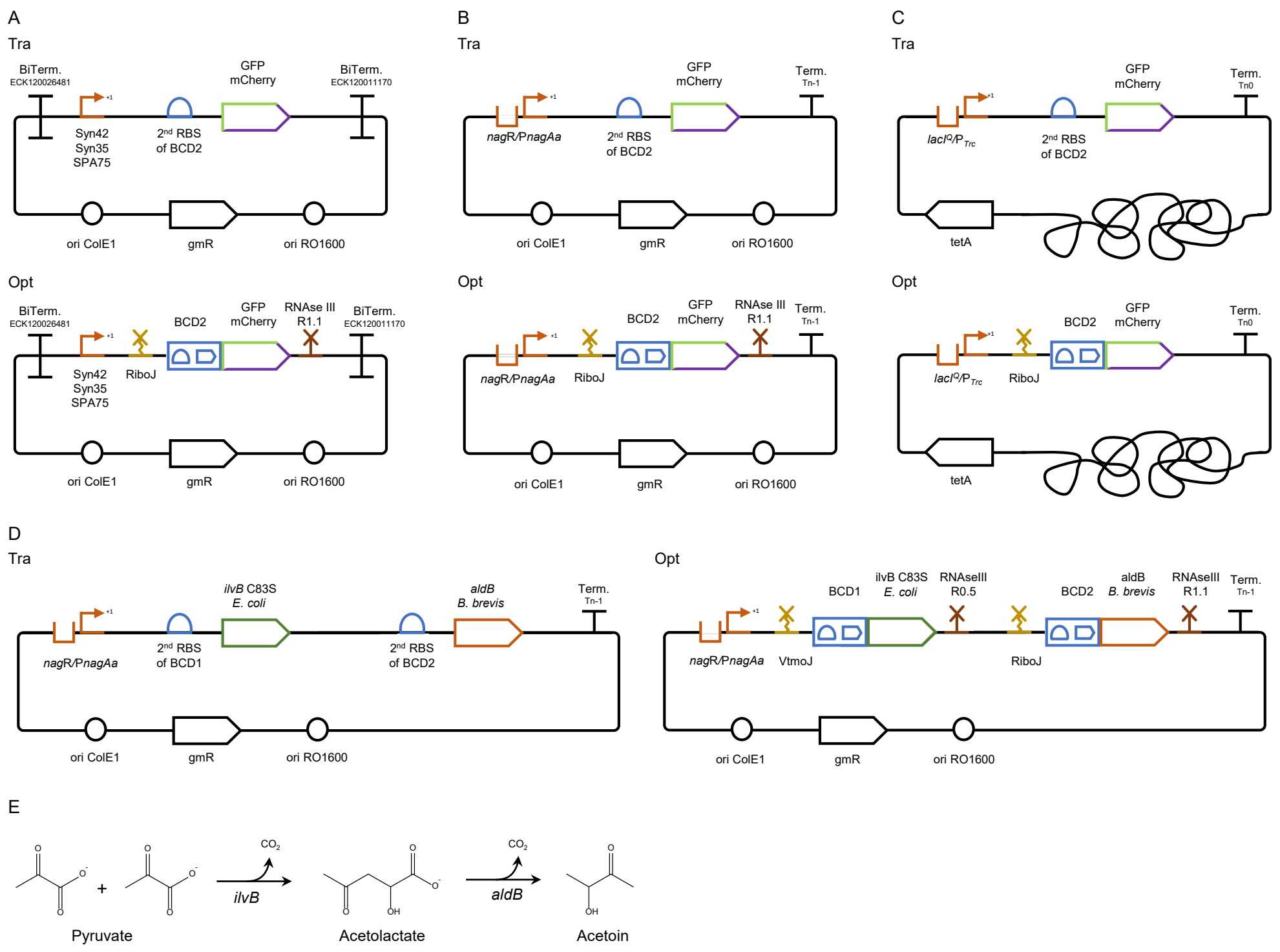
A
Tra
BiTerm.
ECK120026481
GFP
mCherry
BiTerm.
ECK120011170
Syn42
Syn35
SPA75
2nd RBS
of BCD2
ori ColE1
gmR
ori RO1600
Opt
BiTerm.
ECK120026481
BCD2
GFP
mCherry
RNAse III
R1.1
BiTerm.
ECK120011170
Syn42
Syn35
SPA75
RiboJ
ori ColE1
gmR
ori RO1600
B
Tra
GFP
mCherry
Term.
Tn-1
nagR/PnagAa
2nd RBS
of BCD2
ori ColE1
gmR
ori RO1600
Opt
BCD2
GFP
mCherry
RNAse III
R1.1
Term.
Tn-1
nagR/PnagAa
RiboJ
ori ColE1
gmR
ori RO1600
C
Tra
GFP
mCherry
Term.
Tn0
lacIQ/PTrc
2nd RBS
of BCD2
tetA
Opt
BCD2
GFP
mCherry
Term.
Tn0
lacIQ/PTrc
RiboJ
tetA
D
Tra
ilvB C83S
E. coli
aldB
B. brevis
Term.
Tn-1
nagR/PnagAa
2nd RBS
of BCD1
2nd RBS
of BCD2
ori ColE1
gmR
ori RO1600
Opt
BCD1
ilvB C83S
E. coli
RNAseIII
R0.5
BCD2
aldB
B. brevis
RNAseIII
R1.1
Term.
Tn-1
nagR/PnagAa
VtmoJ
RiboJ
ori ColE1
gmR
ori RO1600
E
CO2
ilvB
CO2
aldB
Pyruvate
Acetolactate
Acetoin

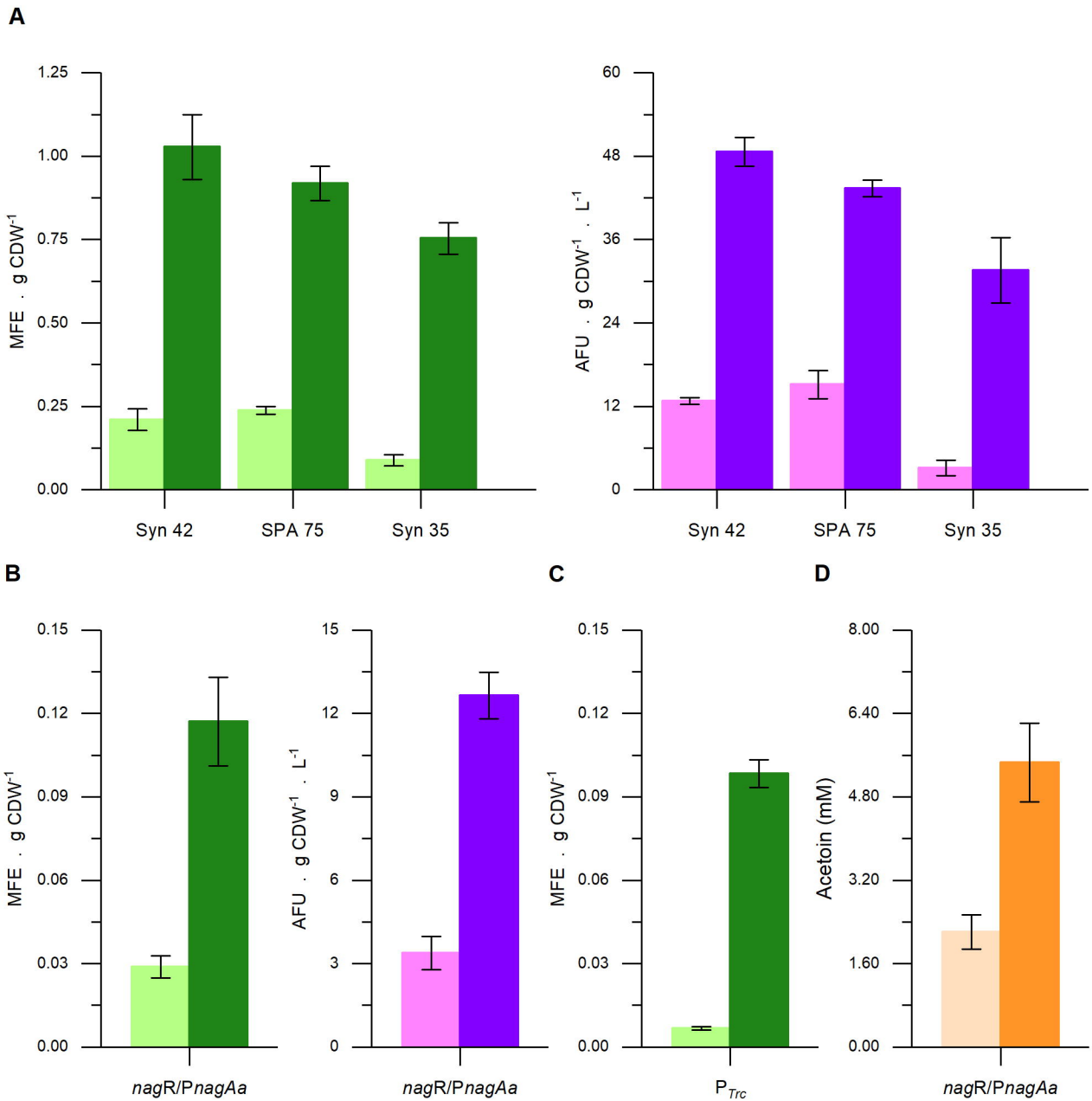
A
MFE . g CDW-1
1.25
1.00
0.75
0.50
0.25
0.00
Syn 42
SPA 75
Syn 35
AFU . g CDW-1 . L-1
60
48
36
24
12
0
Syn 42
SPA 75
Syn 35
B
MFE . g CDW-1
0.15
0.12
0.09
0.06
0.03
0.00
nagR/PnagAa
AFU . g CDW-1 . L-1
15
12
9
6
3
0
nagR/PnagAa
C
MFE . g CDW-1
0.15
0.12
0.09
0.06
0.03
0.00
PTrc
D
Acetoin (mM)
8.00
6.40
4.80
3.20
1.60
0.00
nagR/PnagAa

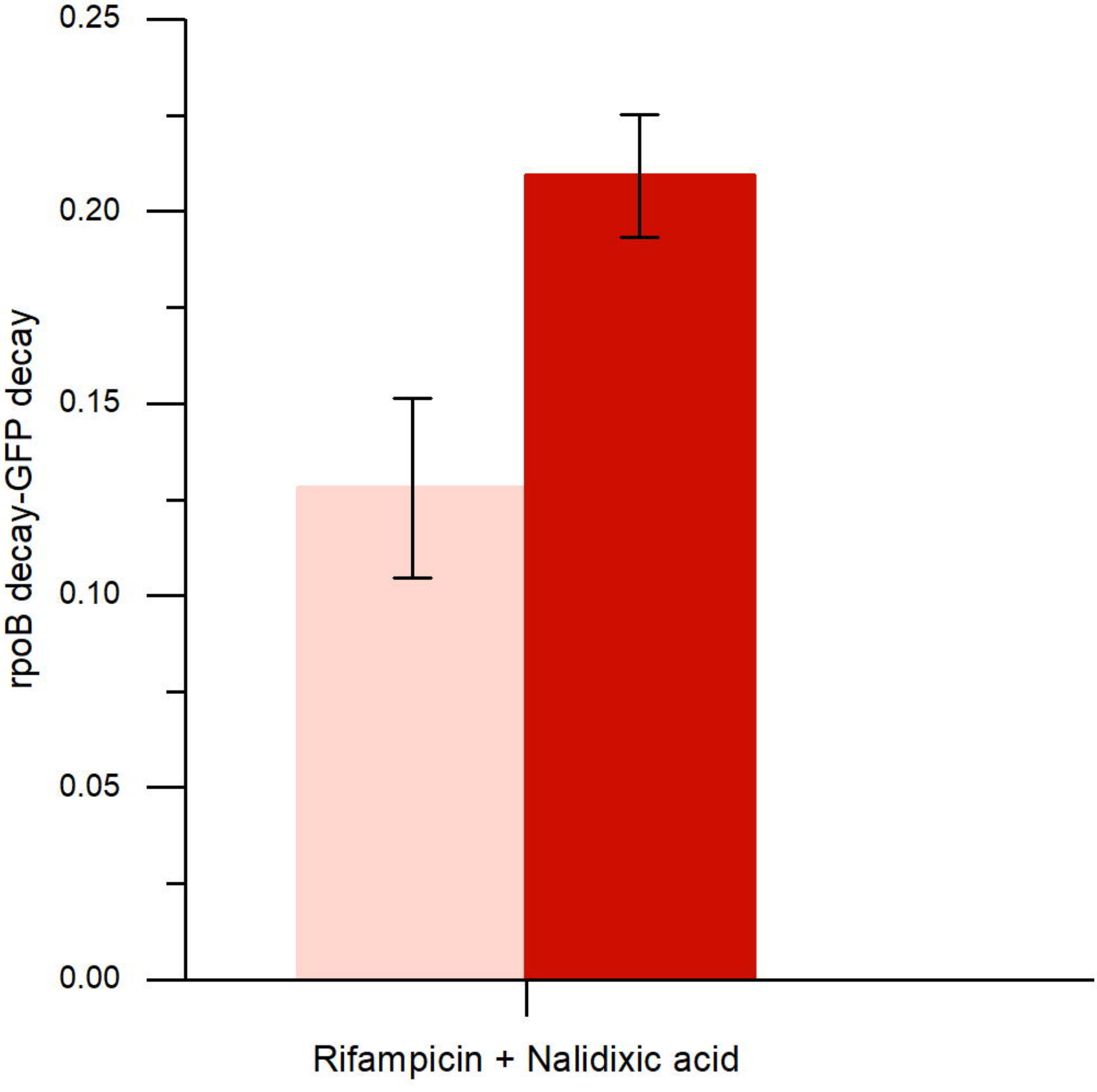
0.25
0.20
0.15
0.10
0.05
0.00
rpoB decay-GFP decay
Rifampicin + Nalidixic acid